Microfluidics and Nanofluidics (2019) 23:70
https://doi.org/10.1007/s10404-019-2238-6

SHORT COMMUNICATION

Characterization of glass frit capillary pumps for microfluidic devices

Matthew Rich[1] · **Omar Mohd**[1] · **Frances S. Ligler**[1] · **Glenn M. Walker**[2]

Received: 11 October 2018 / Accepted: 5 April 2019 / Published online: 11 April 2019

Abstract
Here, we report on a low-cost, disposable microfluidic pump made from sieved glass particles. The pump overcomes the limitations of other passive pumping methods and can handle whole blood, which makes it useful for point-of-care diagnostics. Flow rates of up to 8.7 µL/s and pumping volumes of up to 1 mL were demonstrated, but both can be adjusted by changing pump geometry and particle size. Finally, we demonstrate utility of this pump by attaching it to a commercially available point-of-care immunoassay system from mBio Diagnostics and demonstrating improved binding efficiencies with flow.

Keywords Porous · Glass · Capillary forces · Pump · Microfluidic · Point-of-care

1 Introduction

Pumps are a vital component of any point-of-care (POC) microfluidic device that requires sample manipulation on-chip. POC devices used in the field require a pump that is low-cost, disposable, low-power, and operable by a user with minimal training (Peeling and Mabey 2010; Chin et al. 2012). These design constraints have led to many creative active and passive pumping strategies for POC devices. Active pumps operate for long periods of time and provide adjustable, precise control of pressure or flow rate. This level of control requires an external power supply and greater expense, making active pumps less attractive for POC applications. In contrast, passive pumps use the intrinsic physical properties of a material or structure to generate flow. While they generally provide less control over flow and pumping time than active pumps, passive pumps often satisfy more of the design criteria for POC devices. A comprehensive list of pumping strategies is beyond the scope of this paper, but passive pumping methods have used suction (Lee et al. 2018), Young–LaPlace pressure (Walker and Beebe 2002), capillary pressure (Zimmermann et al. 2007), evaporation (Zimmermann et al. 2005), degassed PDMS (Liang et al. 2011), and osmotic pressure (Xu et al. 2010) among other strategies. Of all the passive pumping strategies, capillary-based pumps have emerged as one of the most reliable methods for controlling fluid flow in POC applications (Olanrewaju et al. 2018).

Capillary pumps require a substrate with embedded pores sufficiently small to generate the capillary pressures necessary for pumping. Others have patterned porous matrices for passive pumps using microfabrication techniques (Zimmermann et al. 2007; Safavieh et al. 2015). Pumps made with these engineered matrices are an attractive platform for studying how capillary forces can be harnessed to create pumps, but specialized equipment is required for fabrication which increases the per-pump cost. In contrast, paper is an inexpensive and commercially available porous matrix suitable for pumping, but the pore-size distribution can vary from batch to batch. Building on the initial work of others (Chumo et al. 2013; Kokalj et al. 2014; Wang et al. 2010, 2013; Xu et al. 2008), we recently demonstrated design principles for creating shaped paper devices that could be used as inexpensive and programmable pumps for microfluidic devices (Cummins et al. 2017a). However, despite its advantages, paper can have difficulty wicking multiphase fluids, like whole blood, reliably. Others have demonstrated that blood flow in paper is highly variable and requires either pretreatment of the paper or the addition of salt to create a

Electronic supplementary material The online version of this article (https://doi.org/10.1007/s10404-019-2238-6) contains supplementary material, which is available to authorized users.

✉ Glenn M. Walker
gmw@olemiss.edu

[1] Joint Department of Biomedical Engineering, University of North Carolina at Chapel Hill and North Carolina State University, Raleigh, NC 27695, USA

[2] Department of Electrical Engineering, University of Mississippi, Oxford, MS 38677, USA

hypotonic solution (Berry et al. 2016; Noiphung et al. 2015). Whole blood samples are attractive for use in POC devices, because they eliminate the expense and processing steps needed for producing serum or plasma (Lykins et al. 2018; Soleymani et al. 2017). Microfluidic POC diagnostics that use whole blood as a sample matrix could benefit from a pump that possesses the advantages of paper but without the drawbacks of clogging and unreproducible flow.

Here, we report a novel strategy for using shaped assemblies of glass particles or "frit" as disposable capillary pumps that are low-cost and less susceptible to clogging than paper. While porous glass and glass frit have been used for years to create active on-chip electroosmotic pumps (Yao et al. 2003; Wang et al. 2009), fused glass frit has not been explored as a porous matrix for capillary pumps. The glass frit is first sieved to create a narrow distribution of particle sizes, and then fused into the desired shape using a mold and an inexpensive hobby kiln. The resulting pumps contain pores larger than those present in paper, thus providing faster flow rates and less clogging. The glass frit pumps were capable of pumping over 1 mL of fluid at speeds greater than 8 µL/s. As a demonstration of utility, we attached the pumps to a commercially available static immunoassay POC device to generate flow and measured the improvement in binding efficiencies within the immunoassay using whole blood as the sample matrix.

2 Methods

2.1 Glass frit pump fabrication

Pumps were fabricated from commercially available clear Uroboros System 96 FX fine (F2-00-96) and medium (F3-00-96) frit (Uroboros Glass Studios, Portland, OR, USA). Figure 1 shows an overview of the fabrication procedure and pump dimensions. The pump dimensions were chosen to fit the mBio cartridge and permit insertion of the assembly into the mBio reader. The lower size limit for glass frit pumps was determined by the feature resolution within the mold and the glass frit size. The upper size limit for the fused glass pumps was dictated by the size of the mold and kiln. The frit was separated into batches of different particle size: 355–425 µm, 425–500 µm, 500–600 µm, 600–710 µm, and 710–850 µm using multiple sieves (McMaster-Carr, Douglasville, GA, USA). Pumps were made from a single batch of frit by pouring the particles into an array of pump molds machined from 304 non-magnetic steel and then leveling the frit using a razor blade. Boron nitride spray was used as a release agent. The mold was then placed in a Skutt GlassMaster LT kiln (Skutt, Portland, OR, USA) and fired using a pre-programmed schedule (see Supplementary Information). After firing, the pumps were carefully extracted from the mold. Pumps with multilayered volume-control regions were fabricated by stacking single pumps without the neck region on top of a pump with the neck region and firing the stack again using the same recipe as a single pump.

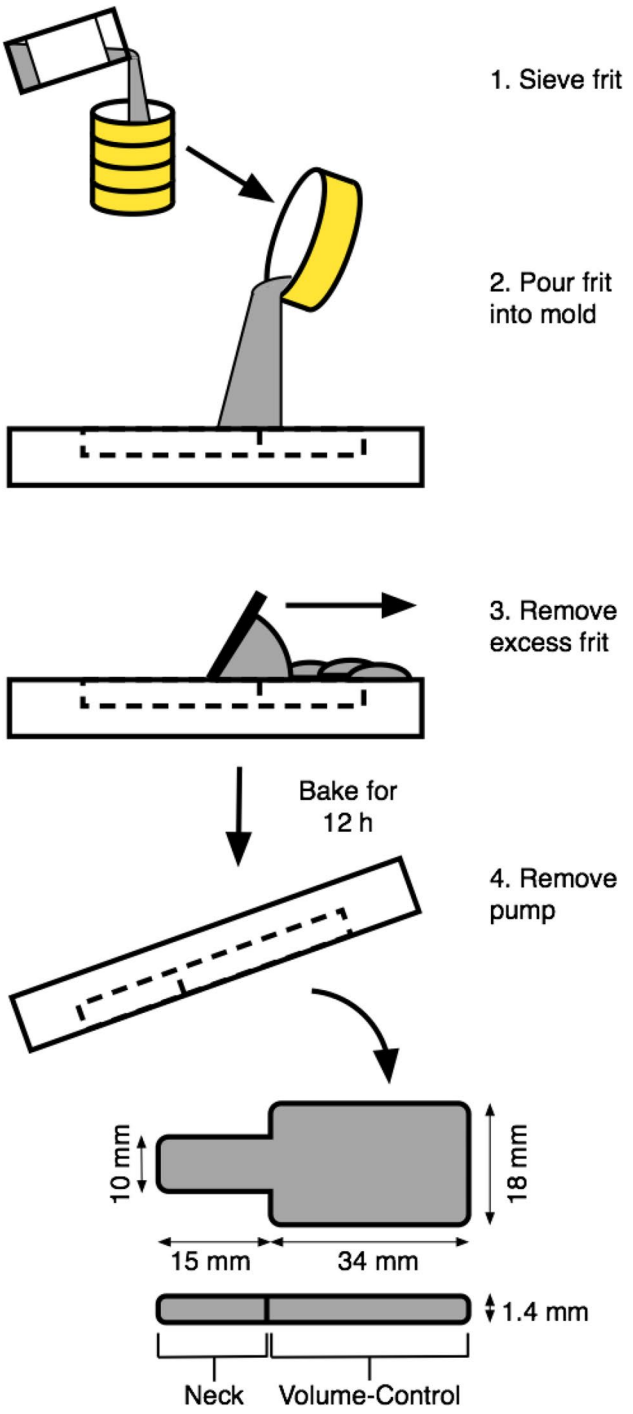

Fig. 1 Glass frit is sieved into different batches. Each batch is then used to fabricate glass frit pumps with a specific range of particle sizes

The rate of pump fabrication is limited only by kiln dimensions. The stainless-steel molds could produce six pumps per firing and the 8″ × 8″ kiln could comfortably accommodate two molds simultaneously. The fabrication procedure yielded pumps with repeatable pore sizes and pumping characteristics. All data are reported in terms of numbers of samples tested ($n = 5$) with the standard deviation of the mean. A new pump was used for each measurement.

2.2 Microfluidic device fabrication

A 3″ × 1″ glass microscope slide (Ted Pella Inc., Redding, CA, USA) served as the base of the simple microfluidic device used for testing blood flow through the pumps. A laser cutter was used to pattern a 5 mm × 54 mm (W × L) microchannel into double-sided adhesive tape (9495B Black, 3M, St. Paul, MN, USA). The tape also defined the microchannel thickness. The microchannel dimensions were chosen to match the microchannel dimensions within the mBio SnapESI cartridges. Inlet and outlet ports were laser-cut into a 3″ × 1″ polystyrene sheet (Goodfellow Corporation, Coraopolis, PA, USA) that was 125 µm thick. The polystyrene sheet, adhesive layer, and glass slide were then stacked and pressed together by hand (see Supplementary Information). Before connecting a pump to the microfluidic device, a 1 mm × 2 mm priming strip of Whatman #1 chromatography paper was first placed in the outlet port of the channel.

Two strategies were used to connect the glass frit pumps to the microfluidic devices. The first approach was to place a ~0.7 mm-thick glass frit puck of diameter 5 mm into the outlet reservoir. The puck was made from frit one sieve size larger than the pump frit to ensure a lower fluidic resistance. A small amount of loose glass frit was placed on top of the puck followed by the fused glass frit pump, completing the assembly. The loose frit was used to ensure hydraulic conductivity between the pump and frit disk. The second approach was to fabricate pumps that contained a puck fused onto the pump neck. Regardless of the approach, the effect was the same and is summarized in Fig. 2. The glass frit pump was placed on top of the microfluidic device and fluid was added to one or more reservoirs attached to the inlet of the microchannel. Fluid from the inlet reservoir filled the microchannel, priming the system. Once the fluid made initial contact with the puck, the hydrophilic porous structure of the pump provided a constant negative pumping pressure until the pump became fully saturated.

2.3 Flow characterization

Volumetric flow rate and pumping volume were measured by weighing the glass frit pumps before and after pumping fluid from the microchannel. Pumps were removed for weighing after 30 s for water and 300 s for blood. The times were chosen to ensure that the pumps were not fully saturated prior to weighing. Masses were converted to volume by assuming $\rho_{water} = 1$ g/cm^3 and $\rho_{blood} = 1.06$ g/cm^3.

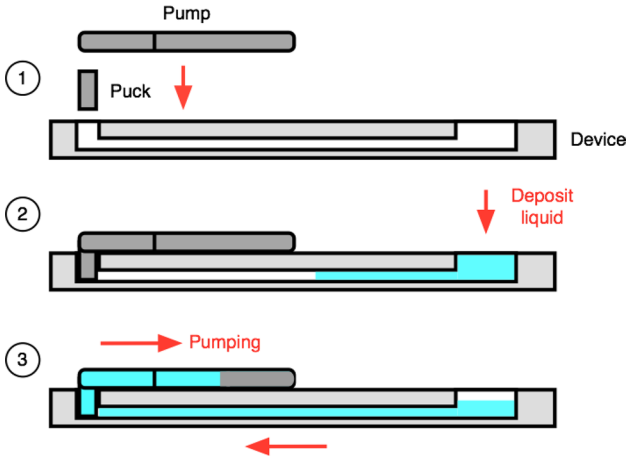

Fig. 2 The glass frit pump is attached to a microchannel prior to priming the device. Capillary forces fill the device and initiate pumping

2.4 Immunoassay characterization

A direct binding assay was used to compare the signal generated by fluorescent antibody binding to immobilized antigens under static vs. flow conditions in whole blood samples. Recombinant llama anti-staphylococcal enterotoxin B (SEB) antibodies A3H2, C8H3, and aad (a kind gift from Dr. George Anderson of the Naval Research Laboratory, Washington, DC, USA), each bearing a His tag to serve as an antigen, were patterned in a 3 × 15 grid on a commercially available optically transparent polymer waveguide (MBio Diagnostics, Boulder, CO, USA) at a concentration of 160 µg/mL. While each of these immunoglobulins displays a His tag, the anti-6X His tag antibody binds with different affinities to the immobilized antigens. Fresh porcine blood mixed with 30 USP of lithium heparin was spiked with anti-6X His tag antibody conjugated to Dylight 650 (ab117504) at a concentration of 0.1 mg/mL. Sample volumes of 75 µL and 750 µL were used for the static and dynamic testing, respectively. The fluorescent signal generated by antibody binding to immobilized antigen was measured using an MBio LightDeck® at 11 equally spaced time points over 10 min.

3 Results and discussion

3.1 Porosity

Porosity was measured by weighing dry and saturated pumps made from glass frit of different sizes. An alternative method

for measuring porosity is to convert the weight of a dry pump to volume and divide by the dimensions of the pump. We did not to use this strategy, because the porous structure of the pumps and the slight unevenness caused by leveling with the razor blade introduced uncertainty in the volume estimation. Instead, each pump was placed on a single microchannel outlet and water was added to the inlet until there was no visible change in inlet water level, indicating that the pump was saturated. The pump was then carefully weighed on a balance. Mass was converted to volume using ρ_{water} and $\rho_{glass} = 2.53$ g/cm^3 (Klein 2015). Once the volume of water, V_W, and the volume of glass, V_G, were known, the porosity, φ, was calculated using the following equation:

$$\varphi = \frac{V_W}{V_W + V_G}. \quad (1)$$

The measured porosities for glass pumps made from a range of glass frit sizes are shown in Fig. 3. The porosity ranged from 0.43 to 0.47 for pumps made from frit sizes ranging from 335–425 µm to 710–850 µm. The results agree with the previous observations that particles of uniform size can be packed to approximately the same degree over a range of particle diameters (Westman and Hugill 1930). While the particles used here were not of uniform size, the size distribution was reduced enough by sieving, such that the particles could be approximated as uniform size. The measured porosities fall near the theoretical maximum porosity of 0.48 achieved when uniform spheres are packed in a regular cubic arrangement (Westman and Hugill 1930). These results suggest that the irregular shapes of the glass frit contribute to inefficient packing, which results in larger void volumes and ensures that pumps of equal size hold approximately the same volume of fluid over a relatively large range of particle sizes.

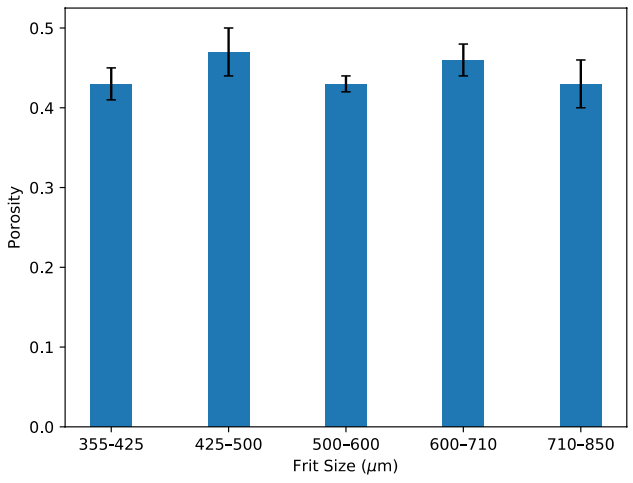

Fig. 3 The total pore volume relative to the pump volume remains within a narrow range regardless of frit size. Values are mean ± SD ($n = 5$)

3.2 Flow characterization

While inefficient packing may produce total void volumes that do not change significantly with average frit size, the range of pore sizes within fused pumps differ. Since porous materials frequently contain a range of pore sizes that pump at different rates within a single material (Cummins et al. 2017b), it is critical to examine the impact of frit size on flow rate and saturation volume. The impact of pore size on flow would also be expected to depend on the viscosity of the fluid being pumped.

The data in Fig. 4a show that the type of fluid plays a critical role in pumping performance. On average, the pumps generated about 10× higher volumetric flow rate for water than blood. Despite the lack of a uniform front often seen in paper during filling (Fig. 4b, c), the flow rates generated by the pumps for each frit size pumps were repeatable. As glass frit size increases, so does the average pore size, which increases the volumetric flow rate. The increase in volumetric flow rate can be explained using the Lucas–Washburn equation $L^2 \sim rt$, where L is the liquid front position, r is pore radius, and t is time. The Lucas–Washburn equation assumes a single pore size and inaccurately predicts the liquid front position in paper (Cummins et al. 2017b). However, the equation is derived from first principles and can be used to establish a square-root relationship between volumetric flow rate and average pore radius. The distance, L, that the liquid front travels is proportional to the volumetric flow rate Q. Therefore, the Lucas–Washburn equation can be re-written as $Q^2 \sim rt$, and predicts that, as r increases, the flow rate will increase to the one-half power. The data in Fig. 4a were fit to curves of the form $Q = \sqrt{rt}$. The measured values for flow rate fit this trend, with $R^2 = 0.87$ and $R^2 = 0.62$ for water and blood, respectively.

Using water, we measured a volumetric flow rate of $Q_0 = 6.4$ µL/s for the 355–425 µm frit size range, which should produce the smallest pore size. We assume that the pores in pumps made from the 710–850 µm frit size have approximately twice the radius of pores in pumps made from the smallest frit. Under this assumption, Lucas–Washburn predicts that the volumetric flow rate for the 710–850 µm frit size range pumps should be $\sqrt{2} \times Q_0 = 9.05$ µL/s. We measured $Q = 8.7$ µL/s, which is in good agreement with the predicted value. The observed values for the intermediate frit sizes also agree well with the predicted values.

With increasing frit sizes, blood pumping rates showed the same upward trend as water. With the smallest frit size pumps, we measured $Q_0 = 0.40$ µL/s, and with the largest, $Q = 0.63$ µL/s. The predicted increase in flow rate for the

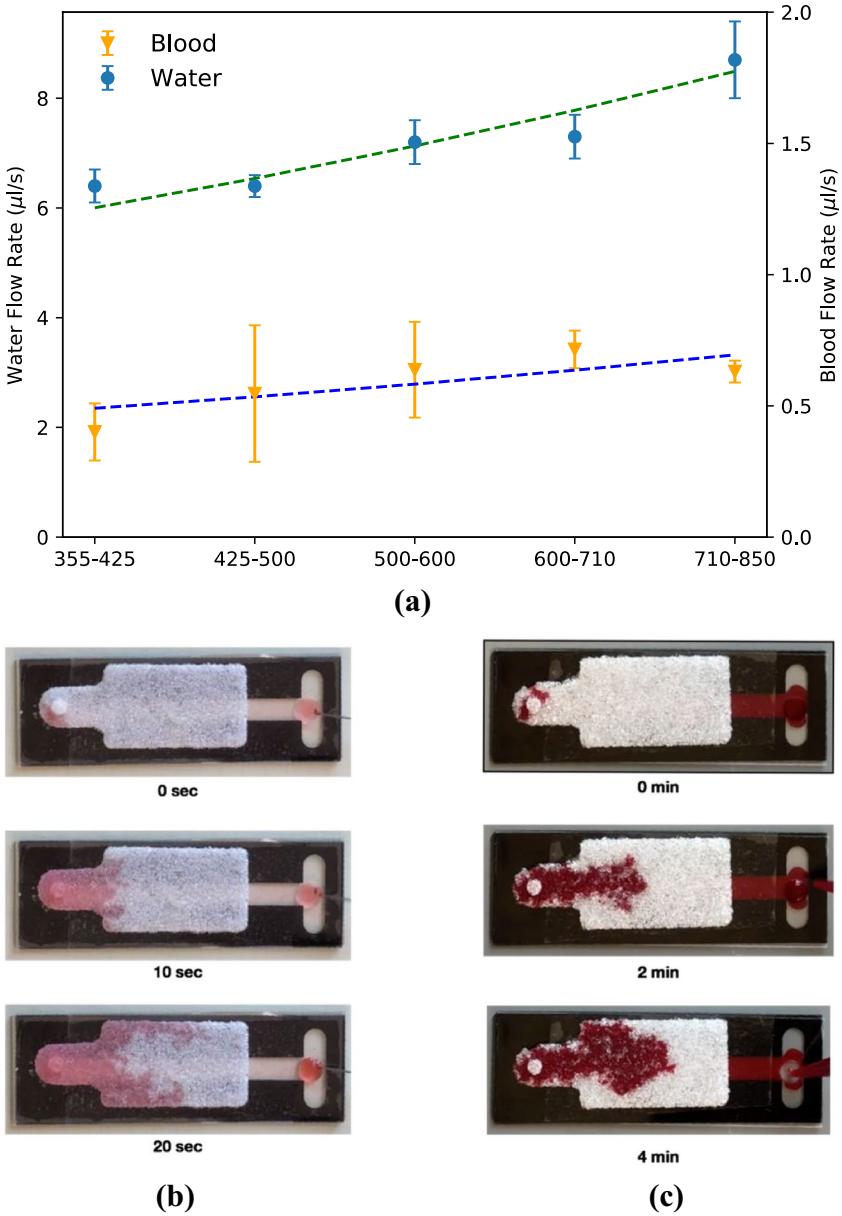

Fig. 4 **a** Average volumetric flow rates of water and blood in pumps made from glass frit of different diameter ($n=5$). Dashed lines show the predicted trend for each set of data. **b** Water with red food coloring filling a pump made from 500 to 600 μm size frit. **c** Blood filling a pump made from 600 to 710 μm frit (color figure online)

largest pore size is $\sqrt{2}\times Q_0 = 0.57$ μL/s, which is in good agreement with the experimentally observed value. The dramatically slower flow rates observed with blood compared to water are likely due to changes in surface tension and red blood cell settling, both of which will affect blood flow within a porous matrix. The surface tension of blood is dependent on protein concentration and red blood cell aggregation at the air–liquid interface, which can vary over time within the pump. As the surface tension changes, the capillary pressure will also change which will affect the flow rate within the pump. In addition, it is likely that large numbers of red blood cells are settling within the porous structure of the pump, clogging fluid paths, and increasing the flow resistance. The forward velocity of blood in the pump with the largest pore size is on the order of 50 μm/s, while the settling velocity of red blood cells is ~ 10 μm/s. The magnitude of settling compared to forward velocity suggests that red blood cells are settling throughout the porous glass pump and altering flow. Both of these processes are stochastic and would explain the slower flow rates observed with blood. We observed maximum pumping time durations of approximately 15 min with blood in the glass frit pumps.

Percolation theory can be used to characterize the filling of porous media with blood and water through the capillary number, $C = V\mu_b/\sigma$, and the ratio of the viscosities of the immiscible fluids within the porous media, $M = \mu_b/\mu_a$ (Lenormand et al. 1988). The velocity of blood within the porous matrix, $V = 100$ μm/s, was estimated from the volumetric flow rate data in Fig. 4a and the known channel and glass frit pump dimensions. The viscosity of blood was assumed

to be $\mu_b = 3$ cP and the interfacial tension of blood with air $\sigma = 0.055$ N/m (Hrncír and Rosina 1997). The viscosity of air was assumed to be $\mu_a = 0.019$ cP. Within the glass frit, blood is the wetting fluid and air is the non-wetting fluid. We calculated log $M = 2.2$ and log $C = -5.3$ for blood, which suggests that filling will occur via capillary fingering. Water has the same order of magnitude viscosity as blood ($\mu_w \sim 1$ cP) and is also a wetting fluid. We calculated M and C values in the capillary fingering regime for water, as well. Figure 4b, c shows capillary fingering produced by water and blood, respectively, as they fill a glass frit pump.

3.3 Volume characterization

Pumps can be stacked to increase the volume of absorbed fluid. Figure 5 summarizes the effect of the number of layers on volumetric flow rate and pumping volume for pumps with only one neck region and additional, stacked volume-control regions. Flow rates for one, two, and three layers were 281, 292, and 275 µL/min, respectively (Fig. 5a). Our earlier work with paper pumps indicated that the higher resistance neck region of the pump controls the flow rate independently from the volume-control region, and these data with glass frit pumps are consistent with those findings (Cummins et al. 2017a). Briefly, the flow rate of fluid into a porous medium slows down, because the fluid must pull itself through an increasing hydraulic resistance as the porous medium wets. However, if the pump is attached to a higher resistance region, such as a pump neck, the flow rate will be constant and controlled by the higher resistance region. The volumetric flow rate can be calculated with $Q = P_c/(R_p(t) + R_n)$, where P_c is the constant capillary pressure within the glass frit, R_p is the pump resistance which changes with time, and R_n is the constant neck resistance. If we assume that the neck resistance is ~ 10× greater than the changing pump resistance, the equation approximates to $Q \sim P_c/R_n$, yielding a constant volumetric flow rate.

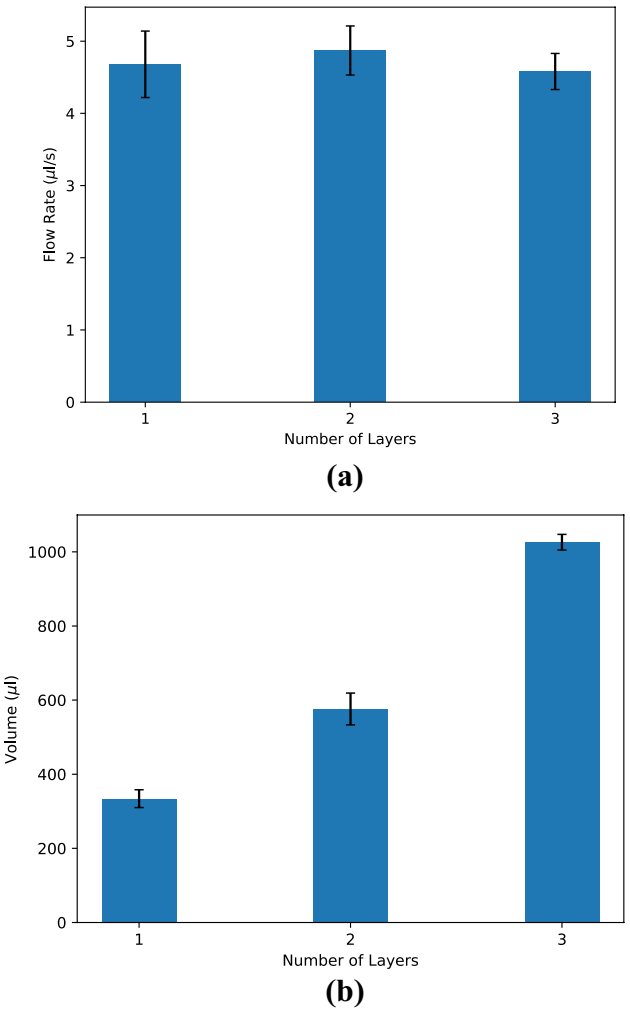

Fig. 5 Pump volume can be increased by stacking multiple pumps. Data are from 425 to 510 µm frit size. **a** The number of layers does not affect the flow rate ($n = 5$). **b** The pumping volume changes linearly ($R^2 = 0.97$) with the number of stacked layers ($n = 5$)

The volume of pumped fluid increases linearly ($R^2 = 0.97$) with the number of layers. Pumped fluid volumes were 334 µL, 576 µL, and 1026 µL, for one, two, and three layers, respectively (Fig. 5b). Since the fabrication mold volume is an unreliable estimate of pump volume, we used the volume from a single-layer pump to estimate the saturation volumes that would be held by two- and three-layer pumps. The neck region accounts for 24% of the total volume of water that can be imbibed into a single-layer pump, and layers two and three lack the neck region. Thus, extrapolating from the data in Fig. 3, the two-layer pump should hold 586 µL and the three-layer pump should hold 857 µL. The predicted volume of the three-layer pump is significantly less than what was measured experimentally. The difference may be caused by surface roughness. After firing, the tops of single-layer glass pumps have more surface roughness than the bottoms, because the tops are not exposed to the mold during firing. When single-layer pumps are stacked, the roughness introduces extra space between the layers which could hold additional liquid volume not predicted by the calculations.

The porosity for twice-fired pumps with one, two, and three layers in the volume-control region was calculated to be 0.38, 0.38, and 0.42, respectively, by comparing the weights of the pumps dry and after full saturation with water. The slightly lower porosities compared to the single-layer, single-fired pumps with porosities of ~ 0.45 (Fig. 3) suggest that the successive firings reduced porosity. The glass frit in the multi-layer pumps was subjected to heating in the kiln twice: once to make each single layer and a second time to fuse the layers together. Multiple firings are likely to reduce the pore volumes within the glass pump, because the glass melts and surface tension causes the frit to fuse further. SEM images in Fig. 6a–c clearly show the particles becoming

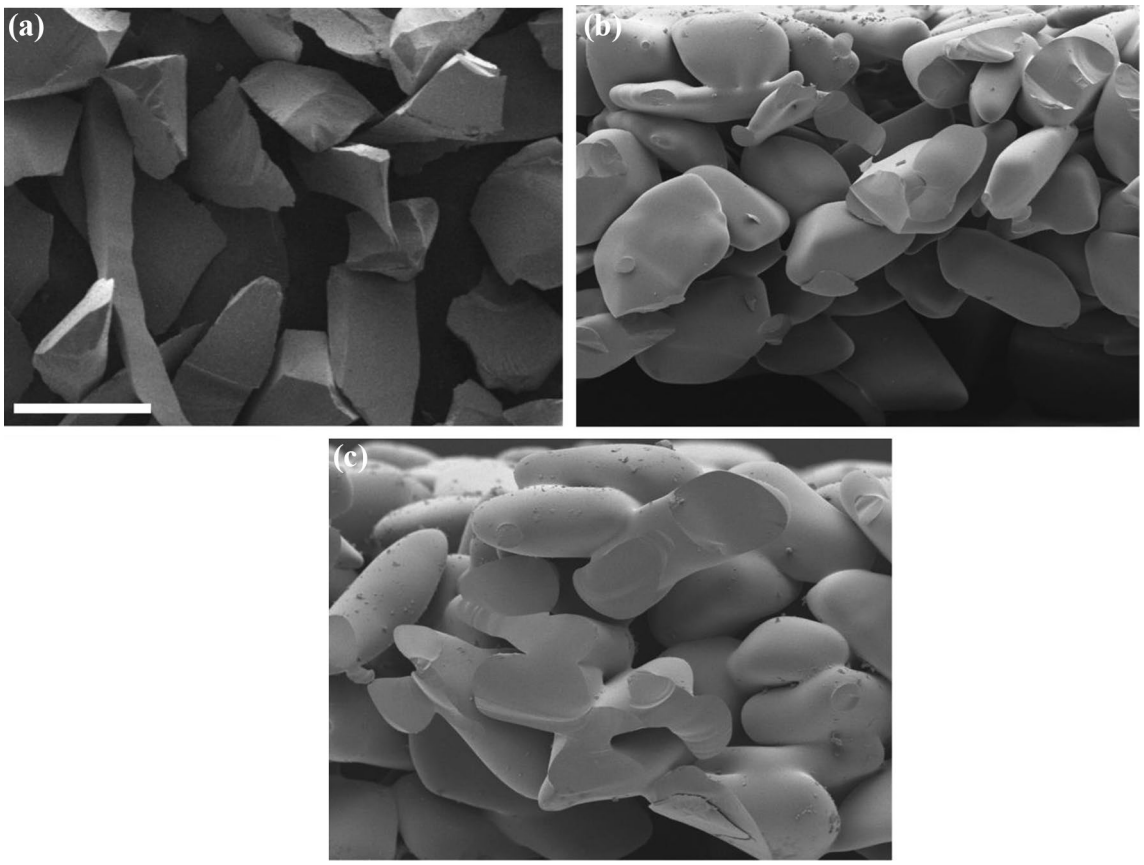

Fig. 6 Scanning electron micrographs showing **a** unfired 425–500 μm glass frit, and a cross section of a pump after **b** one firing and **c** a second firing. The scale bar is 500 μm

more rounded and fusing together, reducing the pore size between particles. While the reduction in pore size can lead to slower pumping rates, the ability to control pore structure could be leveraged to create pumps with tailored porosities for specific applications.

3.4 Immunoassay characterization

We demonstrated how glass frit pumps could be used with whole blood samples in commercially available microfluidic devices by attaching pumps to MBio Diagnostics SnapESI planar waveguide immunoassay cartridges. We hypothesized that attaching a pump to induce flow within the cartridge would increase the flux of a fluorescently labeled IgG antibody to the three different immobilized antigens on the waveguide. Figure 7a–c shows the bound concentration of antibody over time for immunoassays with and without flow. The greatest increase in intensity was measured by antibody binding to the *A3H2* antigen, which had a normalized intensity of 0.12 without flow and 0.24 with flow. In contrast, the smallest increase in intensity was seen with binding of the same antibody to the *aad* antigen, which had an intensity of 0.5 without flow and 0.82 with flow. All immunoassays showed increased intensity under flow conditions, demonstrating that flux to the antigen spots was increased with flow. Normalized intensity did not start at zero, because the microfluidic channel had to be filled with blood prior to insertion into the optical reader. A finite amount of time elapsed before fluorescent intensity measurements began, so some binding occurred before the first measurement was made ($\sim t = 5$ s). Glass frit pumps made from the 810–700 μm particles were used to create average flow rates of 44 μL/min for the immunoassays.

The benefit of flow in improving the assay time and lowering the sensitivity of immunoassays has been theoretically established (Squires et al. 2008). The Damkohler number, *Da*, is a dimensionless number used to determine if a system is reaction-limited or transport (diffusion)-limited. The Damkohler number can be calculated with $Da = k_{on} b_m L/DF$, where $k_{on} = 0.001$ 1/s is the on-rate constant, $b_m = 20{,}000$ sites/μm^2 is the site-binding density, $L = 500$ μm is the characteristic length of the spot containing capture antibodies, $D = 100$ μm^2/s is the diffusion coefficient of the IgG in solution, and $F = 0.81\mathrm{Pe}^{1/3} + 0.7$

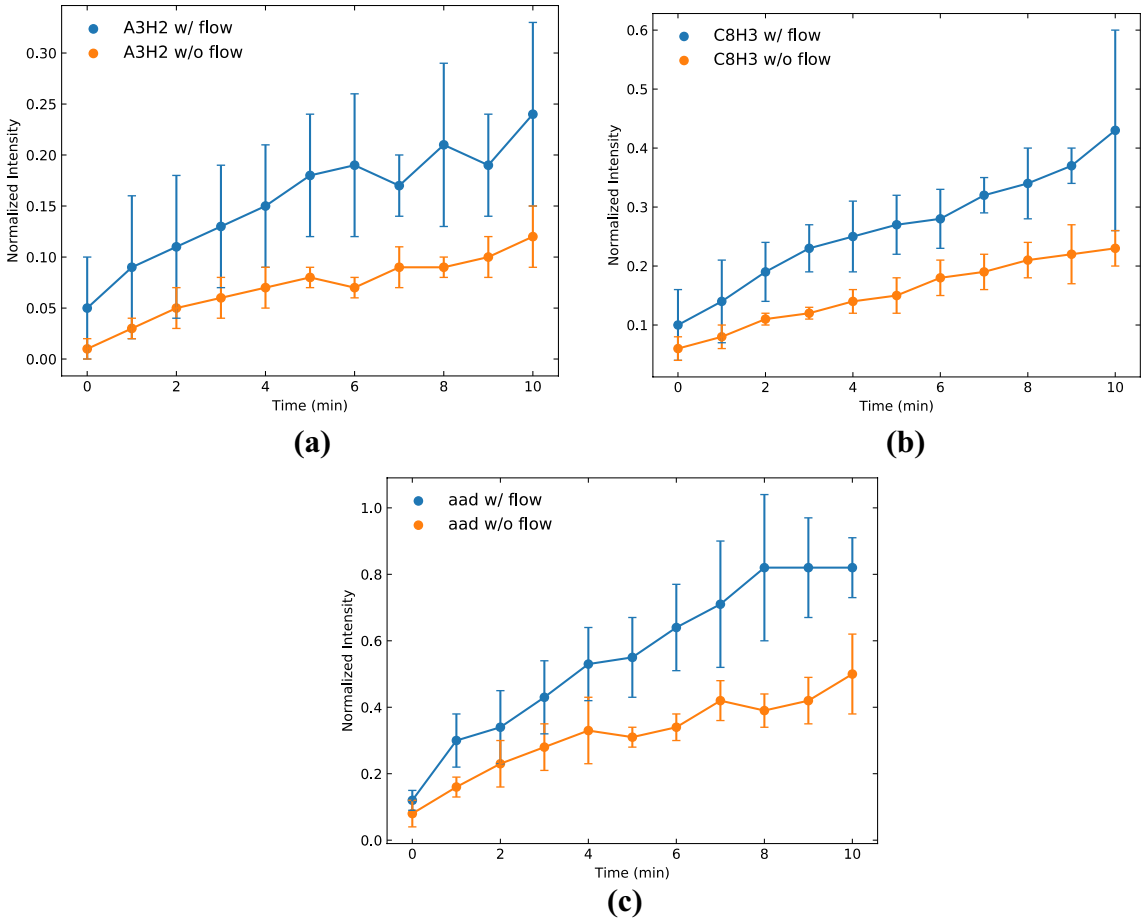

Fig. 7 Flow increases the amount of fluorescent anti-6X His tag antibody bound to **a** *A3H2*, **b** *CBH3*, and **c** *aad* antigens containing terminal His tags ($n=3$) as measured using the MBio Diagnostics system. Static immunoassay results show intensity increasing at a slower rate because of limited diffusive transport

$1\mathrm{Pe}^{-1/6} - 0.2\mathrm{Pe}^{-1/3} = 45.3$ is a dimensionless flux that is a function of the Péclet number of the system. We calculated a Damkohler number of $Da \sim 2$ for the MBio Diagnostics system with a pump attached, meaning that the system was neither strongly reaction-limited nor transport-limited. Even though we saw increased signal from flow, the *Da* number suggests that we could use even faster flow rates before the process becomes reaction-limited. Operating at a higher volumetric flow rate would increase flux to the immobilized antigens in the immunoassay, resulting in a faster time to answer and a lower level of detection. The benefits of using a pump with a microfluidic POC immunoassay will be explored more fully in a future paper.

3.5 Advantages and limitations of glass frit pumps

The key advantage of the glass frit pumps compared to paper pumps is their ability to reliably and repeatedly pump blood. In addition, the flow rate can be tailored by adjusting the glass frit size. However, paper pumps do have some advantages over the glass frit pumps for pumping less complex samples, namely paper pumps are less expensive per pump ($0.07 USD vs. $0.10 USD), and less fragile than the glass pumps. Therefore, glass pumps are an attractive pumping option for whole blood samples in POC devices, while paper pumps may be more appropriate where precise flow control of non-colloidal fluids is required.

4 Conclusion

Porous glass frit pumps are a useful addition to the microfluidic toolbox. The disposable glass pumps overcome several of the limitations of other portable pumps, and their ease of manufacture and controllable pore size make them adaptable to a variety of applications. Glass frit pumps are

made with low-cost off-the-shelf supplies, and the design can be adapted for a variety of footprints, flow rates and flow volumes to facilitate integration with the existing microfluidic devices. The material cost of glass frit pumps could be reduced using semiconductor industry batch-scale approaches for glass frit wafer bonding. Commercial microfluidic devices could incorporate these glass frit pumps, which work well with biological sample matrices like blood, with minimal impact on device cost.

Acknowledgements This work was supported by the North Carolina State University Chancellors Innovation Fund, the North Carolina Biotechnology Center Technology Enhancement Grant, and the Ross Lampe Chair in Biomedical Engineering at North Carolina State University.

References

Berry SB, Fernandes SC, Rajaratnam A, DeChiara NS, Mace CR (2016) Measurement of the hematocrit using paper-based microfluidic devices. Lab Chip 16:3689–3694

Chin CD, Linder V, Sia SK (2012) Commercialization of microfluidic point-of-care diagnostic devices. Lab Chip 12:2118–2134

Chumo B, Muluneh M, Issadore D (2013) Laser micromachined hybrid open/paper microfluidic chips. Biomicrofluidics 7:064109

Cummins BM, Chinthapatla R, Lenin B, Ligler FS, Walker GM (2017a) Modular pumps as programmable hydraulic batteries for microfluidic devices. Technology 5:21–30

Cummins BM, Chinthapatla R, Ligler FS, Walker GM (2017b) Time-dependent model for fluid flow in porous materials with multiple pore sizes. Anal Chem 89:4377–4381

Hrncír E, Rosina J (1997) Surface tension of blood. Physiol Res 46:319–321

Klein J (2015) Additive manufacturing of optically transparent glass. MS Thesis, Massachusetts Institute of Technology, Cambridge, MA, USA

Kokalj T, Park Y, Vencelj M, Jenko M, Lee LP (2014) Self-powered imbibing microfluidic pump by liquid encapsulation: SIMPLE. Lab Chip 14:4329–4333

Lee S, Kim H, Lee W, Kim J (2018) Finger-triggered portable PDMS suction cup for equipment-free microfluidic pumping. Micro Nano Syst Lett 6:1

Lenormand R, Touboul E, Zarcone C (1988) Numerical models and experiments on immiscible displacements in porous media. J Fluid Mech 189:165–187

Liang DY, Tentori AM, Dimov IK, Lee LP (2011) Systematic characterization of degas-driven flow for poly (dimethylsiloxane) microfluidic devices. Biomicrofluidics 5:024108

Lykins J, Li X, Levigne P, Zhou Y, El Bissati K, Clouser F, Wallon M, Morel F, Leahy K, El Mansouri B, Siddiqui M, Leong N, Michalowski M, Irwin E, Goodall P, Ismail M, Christmas M, Adlaoui EB, Rhajaoui M, Barkat A, Cong H, Begeman IJ, Lai BS, Contopoulos- Ioannidis DG, Montoya JG, Maldonado Y, Ramirez R, Press C, Peyron F, McLeod R (2018) Rapid, inexpensive, fingerstick, whole-blood, sensitive, specific, point-of-care test for anti-Toxoplasma antibodies. PLoS Negl Trop Dis 12:e0006536

Noiphung J, Talalak K, Hongwarittorrn I, Pupinyo N, Thirabowonkitphithan P, Laiwattanapaisal W (2015) A novel paper-based assay for the simultaneous determination of Rh typing and forward and reverse ABO blood groups. Biosens Bioelectron 67:485–489

Olanrewaju A, Beaugrand M, Yafia M, Juncker D (2018) Capillary microfluidics in microchannels: from microfluidic networks to capillaric circuits. Lab Chip 18:2323–2347

Peeling R, Mabey D (2010) Point-of-care tests for diagnosing infections in the developing world. Clin Microbiol Infect 16:1062–1069

Safavieh R, Tamayol A, Juncker D (2015) Serpentine and leading-edge capillary pumps for microfluidic capillary systems. Microfluid Nanofluid 18:357–366

Soleymani J, Perez-Guaita D, Hasanzadeh M, Shadjou M, Jouyban A (2017) Materials and methods of signal enhancement for spectroscopic whole blood analysis: novel research overview. Trend Anal Chem 86:122–142

Squires TM, Messinger RJ, Manalis SR (2008) Making it stick: convection, reaction and diffusion in surface-based biosensors. Nat Biotechnol 26:417–426

Walker GM, Beebe DJ (2002) A passive pumping method for microfluidic devices. Lab Chip 2:131–134

Wang X, Cheng C, Wang S, Liu S (2009) Electroosmotic pumps and their applications in microfluidic systems. Microfluid Nanofluid 6:145–162

Wang J, Ahmad H, Ma C, Shi Q, Vermesh O, Vermesh U, Heath J (2010) A self-powered, one-step chip for rapid, quantitative and multiplexed detection of proteins from pinpricks of whole blood. Lab Chip 10:3157–3162

Wang X, Hagen JA, Papautsky I (2013) Paper pump for passive and programmable transport. Biomicrofluidics 7:014107

Westman AR, Hugill H (1930) The packing of particles. J Am Ceram Soc 13:767–779

Xu ZR, Zhong CH, Guan YX, Chen XW, Wang JH, Fang ZL (2008) A microfluidic flow injection system for DNA assay with fluids driven by an on-chip integrated pump based on capillary and evaporation effects. Lab Chip 8:1658–1663

Xu ZR, Yang CG, Liu CH, Zhou Z, Fang J, Wang JH (2010) An osmotic micro-pump integrated on a microfluidic chip for perfusion cell culture. Talanta 80:1088–1093

Yao S, Hertzog DE, Zeng S, Mikkelsen JC Jr, Santiago JG (2003) Porous glass electroosmotic pumps: design and experiments. J Colloid Interface Sci 268:143–153

Zimmermann M, Bentley S, Schmid H, Hunziker P, Delamarche E (2005) Continuous flow in open microfluidics using controlled evaporation. Lab Chip 5:1355–1359

Zimmermann M, Schmid H, Hunziker P, Delamarche E (2007) Capillary pumps for autonomous capillary systems. Lab Chip 7:119–125